

Effect of Fe₂O₃ Addition and Sintering Temperature on mechanical Properties and Translucence of Zirconia Dental Ceramics with Different Y₂O₃ Content

Manuel Fellipe R. P. Alves^a, Sebastião Ribeiro^{a*} , Paulo A. Suzuki^a; Kurt Strecker^b,
Claudinei dos Santos^c

^aUniversidade de São Paulo, Escola de Engenharia de Lorena, Polo Urbo Industrial, Gleba AI-6, 12602-810, Lorena, SP, Brasil

^bUniversidade Federal de São João del-Rei (UFSJ), Praça Frei Orlando, Centro, CEP 36.307-352, São João del-Rei, MG, Brasil

^cUniversidade do Estado do Rio de Janeiro, Faculdade de Tecnologia de Resende, Rodovia Presidente Dutra km 298, Polo Industrial de Resende, 27537-000, Resende, RJ, Brasil

Received: September 03, 2020; Revised: December 14, 2020; Accepted: January 19, 2021

The influence of Fe₂O₃ additions on the microstructure, mechanical properties and translucence of zirconia with 3 mol-% or 5 mol-% Y₂O₃ was evaluated. Samples were pressed with different thickness and sintered at 1475, 1500, 1550 and 1600°C for 2 h. Density, phases, microstructure, roughness, strength and translucency were analyzed. All samples showed densification greater than 99%. After sintering at 1600°C, the phase analysis revealed only tetragonal ZrO₂ in samples with 3% Y₂O₃, while in samples with 5% Y₂O₃ the cubic ZrO₂ phase was identified. Significant increase in the grain size was noted, when increasing the Y₂O₃ content from 3% to 5% from 0.8 μm to 2.3 μm for sintered samples at 1600°C. The strength was affected with Y₂O₃ content and no relevant influence of the Fe₂O₃ on density, microstructure or mechanical properties. Visible reflectance spectroscopy analyses, related to the CIELab scale, indicate variation in the contrast ratio as function of thickness of samples and coloring agent Fe₂O₃ content.

Keywords: dental materials, yttria-stabilized zirconia ceramics, Fe₂O₃, optical properties, flexural strength.

1. Introduction

Over the past few decades, the demand for dental prostheses an aesthetic appearance of natural teeth has stimulated an intense technological rush to replace the metallic infrastructure in prostheses¹. In this scenario, structural ceramics emerged as potential substitutes and so-called “metal free” prosthesis systems have been developed entirely composed of ceramic materials².

Among ceramics applied in dentistry, zirconia, ZrO₂, stands out due to its excellent mechanical properties, such as high fracture toughness and bending strength, as well as being biologically inert¹⁻³. In particular, ZrO₂ stabilized with 3 mol% Y₂O₃, technically known as 3Y-TZP, exhibits outstanding mechanical properties due to the stabilization of the tetragonal phase. This phase, t-ZrO₂, is metastable at room temperature and may undergo transformation into the stable, monoclinic phase, in the wake of a tensile stress field of a crack. This transformation is accompanied by a volume change in the order of 4% to 5%, creating itself compressive stresses in the matrix, which hinders crack propagation and resulting in the highest fracture toughness of all ceramic materials⁴⁻⁶.

One of the best-performing manufacturing processes for manufacturing dental prostheses, in terms of speed and precision, is CAD-CAM milling, computer-aided design (CAD) computer-aided manufacturing (CAM). In this process, the geometry of the prostheses is detailed by a software and pre-sintered, still porous and low strength zirconia blocks are automatically milled^{7,8}. After milling, the prostheses are subjected to a second sintering cycle, aiming at eliminating porosity and maximizing mechanical and aesthetic properties.

The adjustment of color shades of zirconia to natural teeth occurs by adding metal oxides as coloring agents such as Fe₂O₃, CeO₂, Er₂O₃, Bi₂O₃ and MnO₂. Two processing routes are commonly employed⁹: the oxides are added to the starting powder, homogenized, compacted and pre-sintered and then directed to milling, or pre-sintered zirconia blocks are infiltrated with a solution of the coloring agents. However, the infiltration method is less effective because it generates zones with different concentrations of the solution and consequently different shades of color throughout the same block^{9,10}.

Although 3Y-TZP has exceptional mechanical properties, the low translucency of the anisotropic tetragonal phase, prevents an imitation of natural teeth by monolithic zirconia ceramics, requiring the application of a covering porcelain

*e-mail: sebastiao@demar.eel.usp.br

layer. However, the mechanical properties of porcelain are inferior than that of the 3Y-TZP core and therefore more prone to failure¹¹. Furthermore, the porcelain cover is applied manually, representing a time-consuming process with little replicability^{4,7}.

Therefore, the production of dental prostheses of monolithic zirconia with a high degree of translucency and a coloration similar to natural teeth would drastically reduce the need for coverings, representing a significant technological advance in relation to the current manufacturing process, both in mechanical performance and in economic viability of the final product^{4,12}.

The literature converges on the parameters that impact the optical properties of monolithic ceramic materials¹³⁻¹⁵. The thickness of the material is undoubtedly the most important parameter for determining the real fraction of light, since the sum of events referring to all other parameters, such as porosity, birefringence and absorption, depends on the thickness^{16,17}. An equation to simulate real online transmission was proposed by Beer – Lambert - Budworth¹⁶, see Equation 1.

$$T = (1 - R) z e^{-(\alpha + S_p + S_b)z} \quad (1)$$

Where “*T*” = transmittance; “*R*” = reflectance; “*α*” = coefficient of absorption intrinsic to the material; “*S_p*” = coefficient of scattering, referring to residual porosity; “*S_b*” = coefficient of scattering referring to grain boundary (by birefringence or a second phase) and “*z*” = thickness.

The initial efforts to increase the translucency in zirconia were aimed at reducing the particle size of the starting powders, thus improving the sintering kinetics. In this way, it was made possible to reduce sintering temperature and firing time, as well as to reduce the porosity of the sintered bodies¹⁸. In parallel, the purity of the starting powder has also been improved minimizing contamination at grain boundaries and increasing the translucency of the blocks¹⁹.

In recent years, some publications have focused on the induction of the cubic phase, through stabilization with 5 mol% of Y₂O₃, as a means of maximizing translucency due to the isomorph characteristic of this phase, as it has a cubic lattice no birefringence is expected^{12,20}. On the other hand, a higher amount of cubic phase diminishes the amount of tetragonal phase, which, in consequence, lowers the mechanical properties¹². However, it is still unclear of how much a higher cubic phase content may improve the translucency of pigmented blocks in detriment of the final mechanical properties.

In this work, the impact of stabilizing ZrO₂ with 3 mol% or 5 mol% of yttrium oxide on the optical, crystallographic and mechanical properties of polycrystalline zirconia, without or with 0.136 wt% of iron oxide as pigment has been evaluated.

2. Experimental Procedure

2.1 Materials

Four different commercial zirconia powders of the TOSOH Corporation – Japan were used in this work, Zpex (G3) and Zpex Yellow (G3Y), stabilized with 3 mol% of

Y₂O₃, designated as G3 and G3Y, and Smile (G5) and Smile Yellow (G5Y), stabilized with 5 mol% of Y₂O₃, designated G5 and G5Y. The “yellow” powders contain also 0.136 wt.% Fe₂O₃ corresponding to the highest iron oxide concentration necessary to imitate the yellowest natural teeth, as described by color scales used in dentistry. The manufacturer data of the powder characteristics are presented in Table 1.

2.2 Processing

Discs (Ø12.5 x 1.3 mm discs) were compacted uniaxially under a pressure of 100 MPa-30s. They were then sintered at four different final sintering temperatures of 1475, 1500, 1550 or 1600 °C, maintaining a 2-hour threshold. The samples was sintered in air, with a heating rate adopted was 2°C/ min, up to 1100°C with an isothermal holding time of 120 min and further heating up to the pre-established final temperature, with a rate of 5°C/min. This rate was also used for cooling down to room temperature.

2.3. Characterizations

The apparent density of the sintered specimens was measured using the Archimedes principle, following the instructions described in the ASTM C373-06 standard²¹. The relative density (%) was calculated by the ratio between the apparent density and the actual density of each studied composition obtained by measuring powder samples of each composition, after a heat treatment at 1600°C-2hr, in a helium pycnometry, Ultrapyc model 1200e.

The identification of the crystal phases was conducted by X-ray diffraction analysis using a Panalytical - Empyriam diffractometer, Cu-Kα radiation (1.5405 Å) in the 2θ range of 10° to 90°, angular step of 0.01° and a counting time of 100s. The diffractograms were compared with standard crystallographic information sheets (CIF), obtained from the database of inorganic crystallographic structures (ICSD) from the online repository administered by the FIZ Karlsruhe - Leibniz institute. To compare the diffraction patterns obtained with the catalog cards, the X'pert Highscore plus (PANalytical) program was used. For the quantitative phase analysis, Rietveld refinement was done using the FullProf program.

The microstructure of the sintered samples was observed by scanning electron microscopy, JEOL -JSM 7100FT, of

Table 1. Physical-chemical properties of starting powder (manufacturer's data).

Characterisite	ZrO2 (3 mol.% Y ₂ O ₃)		ZrO2 (5 mol.% Y ₂ O ₃)	
	Zpex	Zpex yellow	Smile	Smile Yellow
Code	G3	G3Y	G5	G5Y
Average crystallite size (nm)	40	40	90	90
Specific area surface (m ² /g)	13 ± 2	13 ± 2	10 ± 1	10 ± 1
Density (g/cm ³)	6.09	6.09	6.07	6.07
Y ₂ O ₃ (wt.%)	5.2	5.2	9.3	9.3
HfO ₂ + MgO (wt.%)	2.0	2.0	2.0	2.0
Fe ₂ O ₃ (wt.%)	<0.01	~0.18	<0.01	~0.18

polished surfaces. In order to reveal the grain boundaries, the samples were thermally etched at a temperature of 1400°C for 15 min and heating and cooling rates of 20°C/min and 10 °C/min, respectively. After the thermal attack, the sample surfaces were coated with a gold layer of approximately 20 nm, using a BAL-TEC metallizer, mod.MED 020. The determination of the average grain size was done using the *ImageJ* software, measuring a minimum of 700 grains per sintering condition, following the methodology proposed by Peregrina-Barreto et al.²².

The surface roughness of the samples used for determining the bending strength and of the spectrophotometry tests was determined by optical interferometry with a 3D optical profilometer, Zygo, model NewView 7300.

2.3.1 Bending strength

The biaxial flexural strength of sintered samples was determined by the piston on 3 ball (P-3B) method, using a piston and a base with three semi-spheres of high hardness tempered steel, positioned in a circular and equidistant manner with an angle of 120° to each other, supporting the specimens. A thin plastic film was used to reduce the friction between the spheres of the device and the surface of the specimens. The device was then coupled to an universal testing machine, model EMIC-DL10000, and subjected to a loading rate of 0.5 mm/min until rupture of the samples. The bending strength was calculated by the equations presented in the ISO-6872-15 standard²³, for at least 15 samples per condition, and the Weibull modulus *m* and the characteristic strength σ_0 were determined by the two-parameter Weibull statistical approach²⁴, as described by Equation 2.

$$F = 1 - \exp \left[- \left(\frac{\sigma}{\sigma_0} \right)^m \right] \quad (2)$$

where *F* represents the failure probability, σ the bending strength in MPa; σ_0 the characteristic Weibull strength in MPa and *m* the Weibull modulus.

Although the number of samples are relatively low for the Weibulls modulus analysis, *n*=15 instead of *n*=30, turning the coefficient of variation higher than the expectable, with due care and reinforced by other indications this data can be useful for further discussions.

2.3.2 Visible reflectance spectroscopy

The influence of thickness and composition on translucency and color of sintered samples was analyzed using reflectance colorimeter, X-Rite model CF57 / CA, geometry 45/0, following the guidelines of ISO 2471: 2008²⁵, using samples with thicknesses of 0.35 mm, 0.8 mm, 1.0 mm, 1.2 mm and 1.35 mm.

The equipment was powered with a light source based on CIE standards for the CIELab measurement, D65 standard, and standard samples were used for the white (*L* = 97,53; *a* = -0,04; *b* = 1,62) and black (*L* = 18,67; *a* = 0,03; *b* = 0,14) backgrounds. The results obtained were processed using equations that correlate the Lab quantities to obtain the contrast ratio (Equations 3 and 4) and the color difference (Equation 5).

$$CR = \frac{Y_P}{Y_B} \quad (3)$$

$$Y = \left(\frac{L+16}{116} \right) \cdot Y_n \quad (4)$$

$$\Delta E = \left[(L_w - L_b)^2 + (a_w - a_b)^2 + (b_w - b_b)^2 \right]^{1/2} \quad (5)$$

Where: “CR” is contrast ratio; “Y” is spectral reflectance; “L” is luminance; “a” is coordinate “a*”; “b_w” is coordinate “b*” and the *b* and *w* indices are related to the black and white backgrounds, respectively. Also, “Y_n” is the spectral reflectance for light reflected by a diffuser with perfect reflection, illuminated by the same light source as the object = 100; “ΔE” is the color difference.

3. Results and Discussion

3.1 Relative density

The relative density of the samples sintered under different conditions is shown in Figure 1. All samples exhibited relative density greater than 99%, indicating that all sintering cycles were effective in densification of the specimens and that the residual porosity of samples is very low.

The effect of iron oxide (Fe₂O₃) on the densification and grain growth of yttrium-stabilized zirconia (YSZ) has been debated in the literature. Guo and Xiao²⁶ did not detect any statistically relevant variation in the values measured for the relative density of zirconia doped with 3 or 8 mol% of Y₂O₃ compared to doping with up to 2 mol% of Fe₂O₃. The data reported by these authors are in agreement with the results measured in the present study, where a maximum amount of 0.136 wt.% Fe₂O₃ was added, affirming that within the limits of the analysis of this work, no effective variation of relative density was observed.

3.2 Phase composition

Figure 2 shows the X-ray diffractograms of the ZrO₂ samples stabilized with 3 mol.% Y₂O₃ and containing 0.136 wt.% Fe₂O₃, G3Y, sintered at different temperatures, which are similar to white zirconia ceramics.

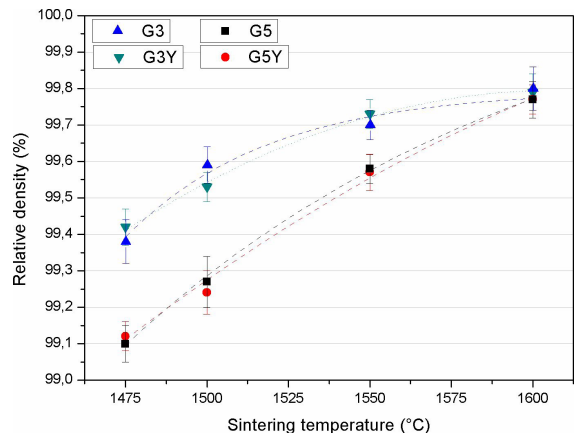


Figure 1. Relative density of zirconia samples sintered at different temperatures.

Qualitatively, all G3Y samples exhibited the tetragonal ZrO_2 phase (spatial group $P42/nmc$) as major crystalline phase. Although the phase diagram presented by Scott²⁷ proposes the existence of a cubic ZrO_2 phase (space group $Fm\bar{3}m$), no trace of this phase could be found in the diffractograms. However, evidence of a secondary crystal phase was observed; see Figure 2b. The peaks of this phase were identified and properly refined as being of a tetragonal ZrO_2 phase (space group $P42/nmc$) with network parameters significantly different from those detected for the main phase and a $c/a\sqrt{2}$ ratio of approximately 1.005, which points to a more stable unit cell, with parameters close to those described for the cubic ZrO_2 phase.

Similar results were reported in previous studies²⁸⁻³⁰, the secondary phase being described as a tetragonal ZrO_2 phase t' , which, although coherent with the space group $P42/nmc$, exhibits a slightly deformed cationic sub-network of fluorite, with oxygen atoms displaced along the “c” axis and not in their preferred positions of the fluorite structure. Lipkin et al.²⁹ and Krogstad et al.³⁰ studied the existence of this tetragonal ZrO_2 t' phase by high-temperature, high-resolution X-ray diffraction (synchrotron radiation) and argued that the phase is the result of regions with a high saturation of Y_2O_3 , but

which still does not have the stability to maintain the fluorite structure, characteristic of the cubic ZrO_2 phase. This phase presents a tetragonality close to that of the cubic ZrO_2 phase but at the same time has a lower Y_2O_3 concentration as expected for the cubic ZrO_2 phase. The X-ray diffractograms of the ZrO_2 samples stabilized with 5 mol.% Y_2O_3 and containing 0.136 wt.% Fe_2O_3 , G5Y, sintered at different temperatures are shown in Figure 3.

Although the phase diagram points out that the composition of the G5Y sample, in the temperature range of the applied heat treatments, is located in a two-phase region, the experimental data obtained point to a three-phase system. Qualitatively, it is possible to infer that the cubic ZrO_2 phase is the major phase, coexisting with a tetragonal ZrO_2 t' phase, of low tetragonality, similar to that identified in the G3Y samples, and the expected tetragonal ZrO_2 phase. Figure 3b clarifies this observation, although the phases have planes at very close 2θ positions. However, in some regions, the peaks were not completely superposed, allowing for an accurate identification of the position of the peaks and the relationship between the network parameters of the phases. Tables 2 and 3 show the results of Rietveld's refinement, according to data published by Kogstad²⁸.

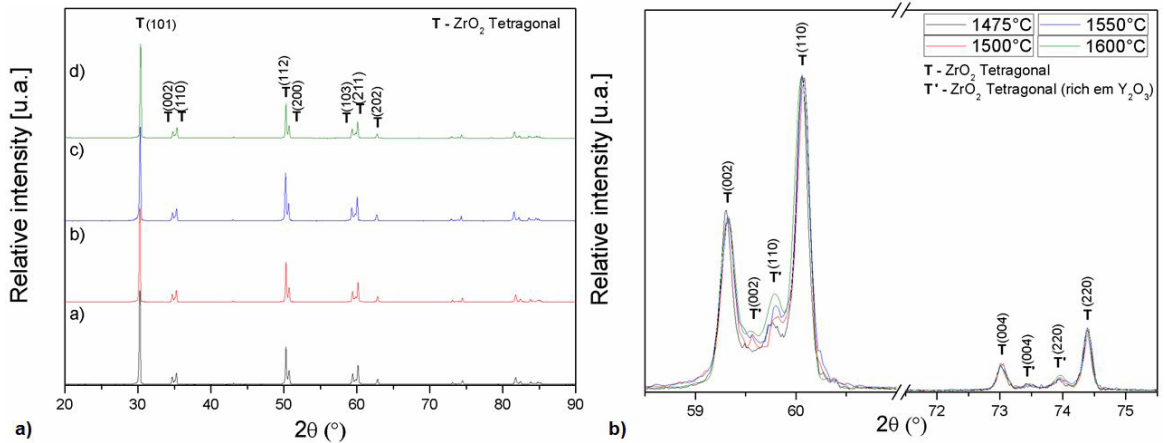


Figure 2. a) X-ray diffractogram of specimens G3Y (ZrO_2 -3mol.% Y_2O_3 + Fe_2O_3) sintered at different temperatures: a) 1475 °C, b) 1500 °C, c) 1550 °C and d) 1600 °C, b) Regions of the diffractograms of the G3Y specimens, indicating the existence of a secondary phase.

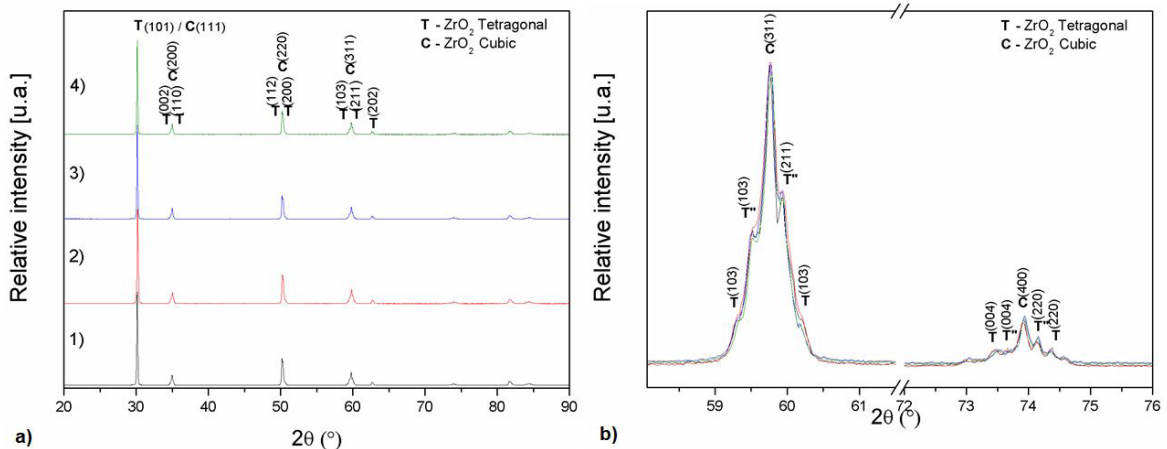


Figure 3. a) X-ray diffractograms of G5Y specimens (ZrO_2 -5mol.% Y_2O_3 + Fe_2O_3) sintered at different temperatures: 1) 1475 °C, 2) 1500 °C, 3) 1550 °C and 4) 1600 °C, b) Regions of the diffractograms of the G5Y indicating the coexistence of three phases.

Table 2. Crystallographic parameters of the G3Y samples (ZrO₂-3mol.%Y₂O₃ + Fe₂O₃) in regard to sintering temperature.

	1475°C	1500°C	1550°C	1600°C
ZrO₂–Tetragonal (ZrO₂ - t)	a = 3.6049 Å	a = 3.6035 Å	a = 3.6031 Å	a = 3.6028 Å
Spacial group	c = 5.1788 Å	c = 5.1780 Å	c = 5.1780 Å	c = 5.1788 Å
P4 ₂ /nmc	V = 67.3001 Å ³	V = 67.2374Å ³	V = 67.2225 ³	V = 67.2217 Å ³
Tetragonality (c/a√2)	10.158	10.161	10.162	10.164
Y₂O₃ content of T-ZrO₂ (mol.%)	2.43	2.35	2.31	2.23
ZrO₂–Tetragonal'' (ZrO₂ - t'')	a = 3.6215 Å	a = 3.6280 Å	a = 3.6220 Å	a = 3.6240 Å
(Yttria rich)	c = 5.1530 Å	c = 5.1600 Å	c = 5.1510 Å	c = 5.1530 Å
Spacial group	V = 67.5829 Å ³	V = 67.9179 Å ³	V = 67.5754 Å ³	V = 67.6763 Å ³
P4 ₂ /nmc				
Tetragonality (c/a√2)	10.061	10.057	10.056	10.054
Y₂O₃ content of the ZrO₂ - t'' phase (mol %)	5.66	5.81	5.84	5.89
Phase composition (wt.%)	82.37% ZrO ₂ -T 17.63% ZrO ₂ -t''	81.25% ZrO ₂ -T 18.75% ZrO ₂ -t''	80.54% ZrO ₂ -T 19.46% ZrO ₂ -t''	79.05% ZrO ₂ -T 20.95% ZrO ₂ -t''
χ²	2.94	3.46	2.73	2.87

Table 3. Crystallographic parameters of the G5Y samples (ZrO₂-5 mol.%Y₂O₃ + Fe₂O₃) in regard to sintering temperature.

	1475 °C	1500 °C	1550°C	1600°C
ZrO₂–Tetragonal (ZrO₂ - t)	a = 3.6040 Å	a = 3.6050 Å	a = 3.6060 Å	a = 3.6064 Å
Spacial group	c = 5.1800 Å	c = 5.1800 Å	c = 5.1800 Å	c = 5.1800 Å
P4 ₂ /nmc	V = 67.2820 Å ³	V = 67.3194 Å ³	V = 67.3567 Å ³	V = 67.3717 Å ³
Tetragonality (c/a√2)	10.163	1.016	1.0157	1.0156
Y₂O₃ content of T-ZrO₂ (% mol)	2.26	2.36	2.45	2.48
ZrO₂–Tetragonal'' (ZrO₂ - t'')	a = 3.6262 Å	a = 3.6238 Å	a = 3.6240 Å	a = 3.6242 Å
(Yttria rich)	c = 5.1530 Å	c = 5.1520 Å	c = 5.1540 Å	c = 5.1551 Å
Spacial group	V = 67.7584 Å ³	V = 67.6557 Å ³	V = 67.6894 Å ³	V = 67.7113 Å ³
P4 ₂ /nmc				
Tetragonality (c/a√2)	10.048	10.053	10.056	10.058
Y₂O₃ content of the ZrO₂- t'' phase (% mol)	6.10	5.94	5.83	5.79
ZrO₂– Cubic (ZrO₂ - c)	a = 5.1394 Å	a = 5.1390 Å	a = 5.1378 Å	a = 5.1370 Å
Spacial group	V = 135.745 Å ³	V = 135.718 Å ³	V = 135.622 Å ³	V = 135.559 Å ³
P4 ₂ /nmc				
Y₂O₃ content of the ZrO₂-c phase (% mol)	7.05	6.92	6.53	6.27
Phase composition (wt.%)	31% ZrO ₂ - t 24% ZrO ₂ - t'' 45% ZrO ₂ -C	30.1% ZrO ₂ - t 23.9% ZrO ₂ - t'' 46% ZrO ₂ -C	27.8% ZrO ₂ - t 26% ZrO ₂ - t'' 46.2% ZrO ₂ -C	27.2% ZrO ₂ - t 25.7% ZrO ₂ - t'' 47.1% ZrO ₂ -C
χ²	2.42	3.31	2.57	2.46

The quantitative phase analysis of the G3Y samples points to a reduction of the content of Y₂O₃ in solid solution of the tetragonal ZrO₂ phase from 2.43 mol.% to 2.23 mol.% with increasing sintering temperature from 1475 °C to 1600 °C. These findings are consistent with the phase transformation mechanism induced by grain contour segregation (GBSIPT) proposed by Matsui³¹. This phenomenon is also accompanied by an increase in tetragonality, expressed by an increase of the c/a√2 ratio, of the tetragonal ZrO₂ phase, due to the concomitant incorporation of anionic vacancies, and a reduction of tetragonality of the tetragonal ZrO₂ t'' phase, as can be verified by diminishing c/a√2 ratios. On the other hand, the G5Y samples, presented a different behavior from the one identified for the G3Y samples: The Y₂O₃-rich, cubic ZrO₂ and t'' tetragonal ZrO₂ phases, showed some loss of Y₂O₃ with increasing sintering temperature, a tendency to stabilize within the analyzed limits was not identified, with a fraction in solid solution slightly higher than 5.8 mol% in samples sintered at 1600 °C. Consequently, the tetragonal ZrO₂ phase showed a slight increase in the Y₂O₃ content, to

values close to those proposed by Scott²⁷ for the stabilization of this phase.

3.3 Microstructural analysis

The microstructures of samples G3Y and G5Y sintered at different temperatures are shown in Figures 4 and 5.

The microstructure of G3Y samples are composed of equiaxed grains with a homogeneous size distribution and essentially pore free. With increasing sintering temperature from 1475°C to 1600°C an increase of the average grain size from 0.55 μm to 0.79 μm can be observed. Some previous studies³²⁻³⁴ analyzed the relationship between an increase of the average grain size and the stability of the t-ZrO₂ phase, and its effect on the mechanical properties of Y-TZP. In this context, Wang and Stevens³² reported results similar to those presented by Zhang¹² and Shahmiri et al.³⁵, regarding the existence of a critical grain size and concluded that samples with an average grain size larger than 1.37 μm showed a reduction in fracture toughness of about 11% and 23.5% in

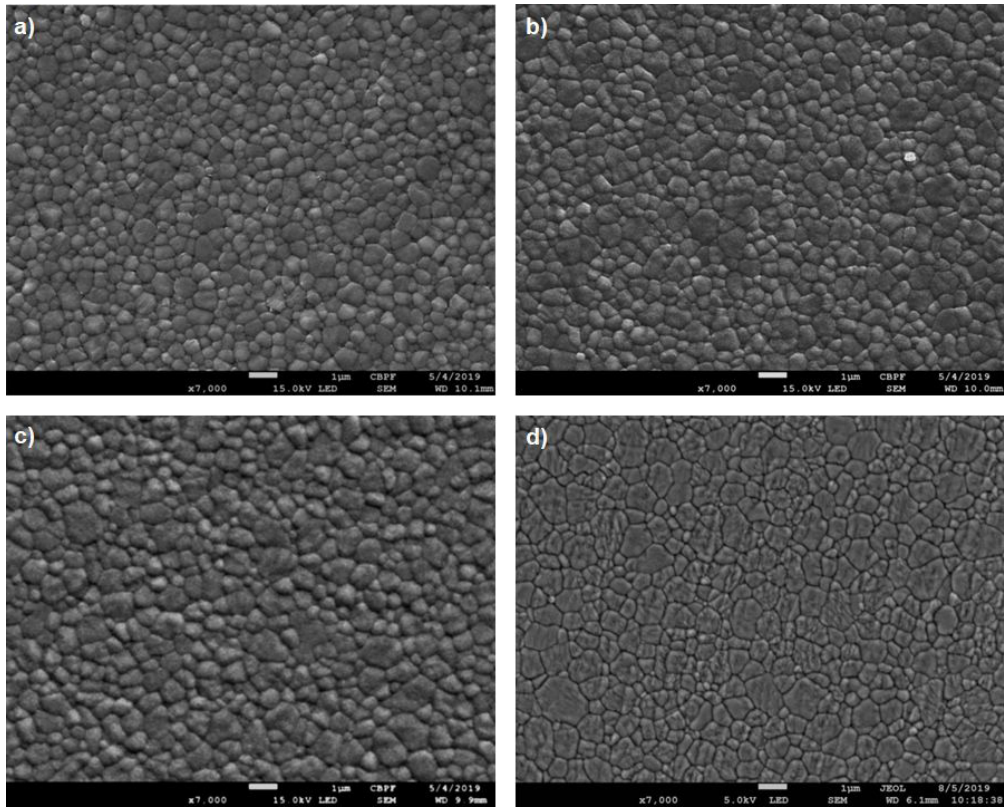


Figure 4. SEM micrographs of G3Y specimens sintered at: a) 1475 °C, b) 1500 °C, c) 1550 °C and d) 1600 °C.

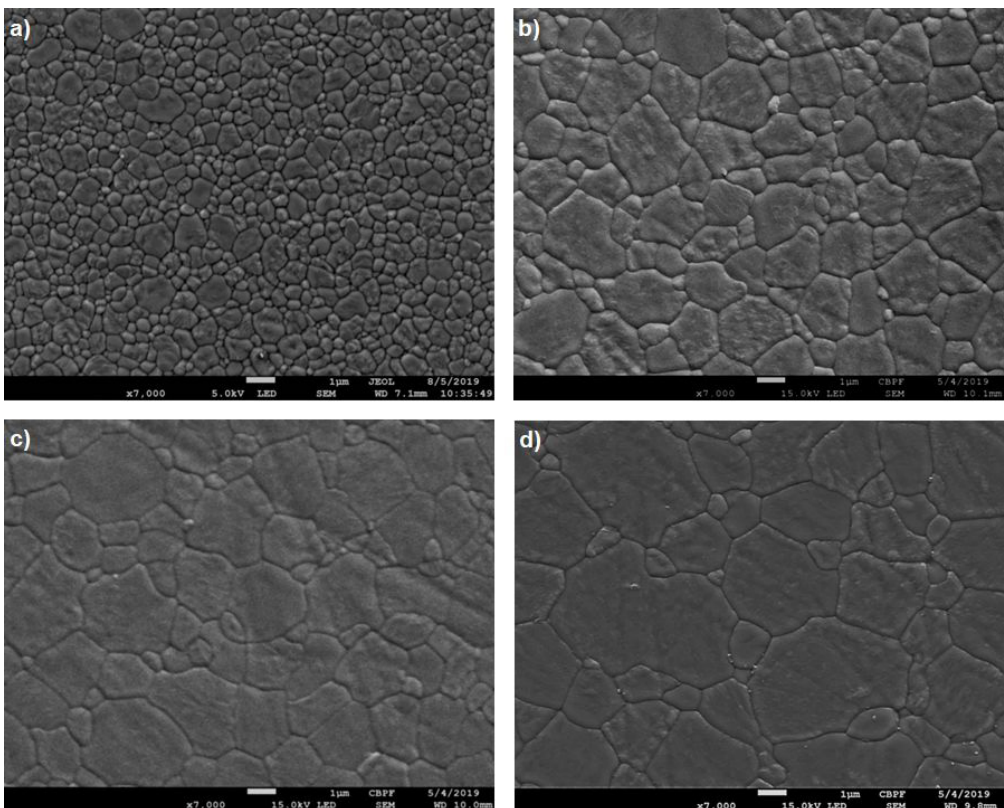


Figure 5. SEM micrographs of G5Y specimens sintered at: a) 1475 °C, b) 1500 °C, c) 1550 °C and d) 1600 °C.

flexural strength. On the other hand, Xue et al.³⁴ analyzed submicrometric microstructures, reported that samples with an average grain size of 0.1 μm to 0.4 μm showed no variation of the mechanical properties, specifically of fracture toughness.

Basu et al.³³ proposed that the increase in grain size can be directly associated with the reduction of free energy of the grain boundary and consequently with a reduction of the metastability of the t-ZrO₂ phase. For the authors, this change in phase stability means that, when exposed to a stress field, even of low intensity, the grains transform almost immediately and subsequently induce the transformation of neighboring grains in an autocatalytic manner, where the transformation of a new grain would be induced by the stress field created by a neighboring grain and not necessarily by the stress field of a propagating crack, resulting in the formation of a larger and more effective transformation zone.

Even so, the effective determination of a possible critical size for the spontaneous transformation of t-ZrO₂ grains is a complex issue, since it depends on multiple factors, such as grain size, Y₂O₃ concentration and residual thermal stresses, which can be affected by the degree of anisotropy, tetragonality, or the existence of secondary phases. Quantitatively, literature points to a critical grain size close to 1 - 1.2 μm ^{12,32,35}. Thus, within the sintering conditions employed in this study, the increase in the average grain size of the G3Y samples will not be prejudicial for the mechanical properties. As we have demonstrated in our recent publication³⁶, working with the same compositional range of Fe₂O₃, the coloring additive did not have a significant impact in the microstructure of the ZrO₂ based ceramics. Based on this, only the SEM's for the colored samples are showed in this manuscript.

On the other hand, samples stabilized with 5 mol.% of Y₂O₃, G5Y showed a significant grain growth, see Figure 5, with increasing sintering temperature from 0.62 μm to 2.32 μm , when sintering at 1475 °C or 1600 °C, respectively, representing an increase of 275%. The grain growth observed for samples of this composition, G5Y, is therefore much higher than that observed for the G3Y samples, under otherwise identical sinter conditions, see Figure 6.

Several authors studied the grain growth kinetics of the cubic ZrO₂ phase as a function of the of the Y₂O₃ content of

the starting powder^{37,38}. In comparison, the authors observed a grain growth for the c-ZrO₂ phase about thirty times greater as for t-ZrO₂, under otherwise identical processing conditions. In the present work, the analyzed micrographs of G5Y samples sintered at 1475°C indicate a homogeneous microstructure of mostly equiaxed grains with a narrow size distribution. However, for sintering temperatures above 1500 °C, a duplex microstructure, composed of a major population of large grains and a second population, of significantly smaller average size, uniformly distributed among the large grains, can be observed.

Matsui et al.³⁹ proposed that the precipitation of c-ZrO₂, rich in Y₂O₃, in a matrix of t-ZrO₂, with a nominal composition of 3 mol% Y₂O₃, occurs through the mechanism described by them as GBSIPT. The solute trawling theory is considered as the driving force of this mechanism, since the diffusion of Y₂O₃ to the grain boundary of two tetragonal grains, leads to the saturation of this region and the nucleation of c-ZrO₂, rich in Y₂O₃, may start.

The measured 3D roughness of the polished surfaces of the G3Y and G5Y samples indicate that the surface finishing of all samples was similar, regardless of the sintering conditions or compositions used. The average Ra parameter, which represents the arithmetic mean of the peaks and valleys, was 26 nm for G3Y samples and 22 nm for G5Y samples, with maximum peak and valley variations of +298 nm / -698 nm for G3Y samples and +302 nm / -278 nm for G5Y samples.

3.4 Bending strength

The results of the bending strength tests are shown in Figure 7. Specimens of G5 and G5Y, presented mean values of flexural strength in the order of 600 MPa, consistent, but close to the minimum requirement for the manufacture of dental prostheses of class 4 ($\sigma \geq 500$ MPa), such as three-element bridges involving molar restoration. However these ceramics are not suitable for the manufacture of class 5 dental prostheses ($\sigma \geq 800$ MPa), such as prostheses of four or more elements. On the other hand, the specimens of G3 and G3Y, presented average values of flexural strength in the order of 1180 MPa, much higher than the requirements for class 5 prostheses.

Typically, ceramic materials exhibit fragile fractures, so failure is usually associated with the presence of a critical size defect, such as a pore or inlay at the sample surface or volume, from where crack propagation will start. Thus, it is expected that the distribution of the measured values for the rupture stress will present an asymmetric distribution, being necessary the use of a non-parametric statistical approach for the adequate understanding of the results. Figure 7b shows the Weibull distribution and failure probability regarding the dispersion of the measured values for each set of samples.

Figure 7b shows that samples without Fe₂O₃ have a higher Weibull modulus, $m \approx 13$, than those containing the coloring agent, $m \approx 8$. The Weibull modulus m describes the shape parameter of the distribution, i.e higher m values correspond to a sharper distribution and therefore also to a higher reliability of the material. Holz et al.⁴⁰ studied the effect of 3Y-TZP doped with up to 0.4% Fe₂O₃, noting that the flexural strength in the order of 1100 MPa was not significantly affected by the Fe₂O₃ additions. However,

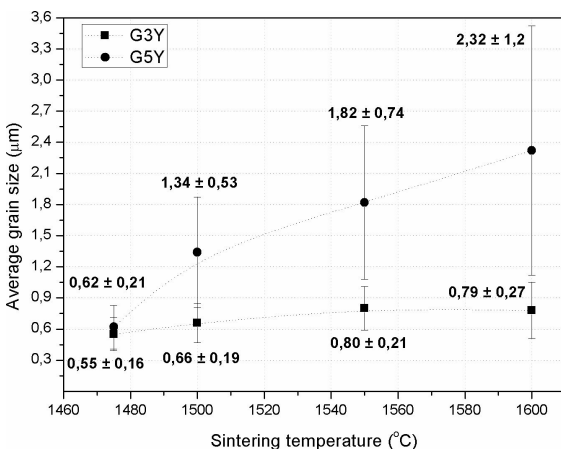


Figure 6. Average grain size as a function of sintering temperature for samples G3Y and G5Y.

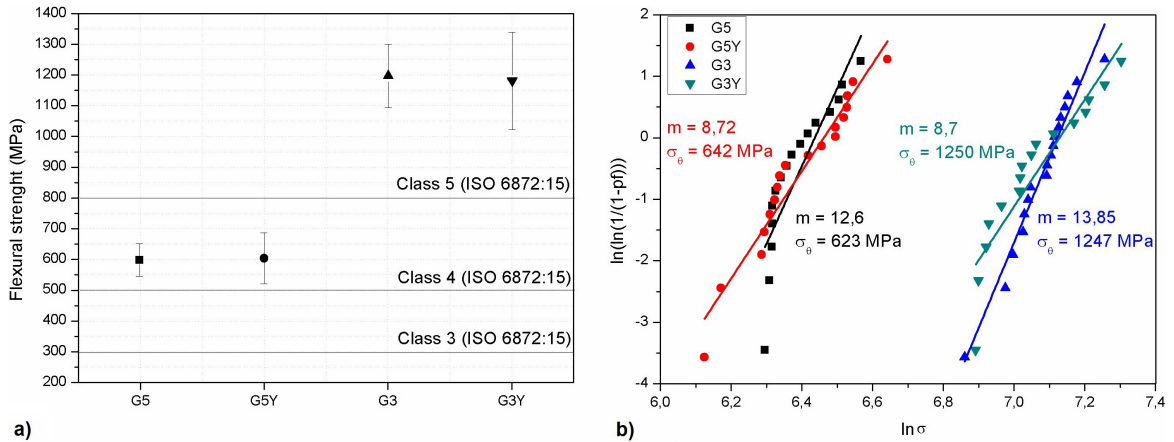


Figure 7. a) Flexural strength of samples G3, G5, G3Y and G5Y sintered at 1500 °C - 2h; b) Weibull modulus of the sintered samples.

the authors did not consider Weibull's statistical analysis when processing the results, and there are no records in this regard. Sedda et al.⁴¹ analyzed bleached, pre-colored and colored blocks when pre-sintered, with the use of coloring liquids. The authors also did not detect any variation in the average strength results, in the order of 1270 MPa. However, the Weibull modulus measured for the samples without color ($m = 16.8$) was significantly higher than that of the pre-colored samples ($m = 12.5$), indicating a wider spread of results for this group. This tendency is similar to the observations made in the present work.

The results of the characteristic strength σ_0 of the Weibull analysis, corresponding to the stress level at which failure probability is 63.21%, are also presented in Figure 7b. The characteristic strength σ_0 is similar for samples stabilized with the same amount of Y_2O_3 , independent of the doping with the coloring agent Fe_2O_3 , that is samples G3 and G3Y, containing 3 mol% Y_2O_3 showed characteristic strengths of 1247 MPa and 1250 MPa, respectively, while samples G5 and G5Y showed characteristic strengths of 623 MPa and 642 MPa, respectively. However, the characteristic strength varied significantly when comparing samples stabilized with 3 mol.% or 5 mol.% of Y_2O_3 , with a variation of about 100%. On the other hand the Fe_2O_3 of 0.136 wt.% had almost negligible effect on characteristic strength, showing a variation of 3% for samples containing 5 mol.% Y_2O_3 and a variation of only 0.25% for samples containing 3 mol.% Y_2O_3 . This information reinforces the premise that the amount of Fe_2O_3 was too low to affect the mechanical properties of the studied ceramic materials in a significant manner.

3.5 Optical properties

The results of the optical properties are discussed according to the contrast ratio, which considers only the results computed for the luminance axis (L), and the color difference.

3.5.1 Contrast ratio

Figure 8 shows a comparison between the contrast ratio (CR) of specimens G3 and G5, sintered at different temperatures, depending on the thickness of the analyzed specimens.

The results indicate a tendency decreasing translucency and an increase in the contrast ratio, with increasing sample thickness. This behavior is explained by the strong correlation between sample thickness and the number of possible scattering events. The formalism of this trend is explained in several models dedicated to the description of optical behaviors, as described by Equation 4^{12,42-44}.

$$T = (I - R)^2 e^{-(\alpha + S_p + S_b)^t} \quad (4)$$

where: "T" is transmittance; "R" is reflectance; " α " is absorption coefficient intrinsic to the material; " S_p " is scattering coefficient due to secondary phases and porosity; " S_b " is spreading coefficient due to birefringence and "t" is thickness.

Another trend observed is the relationship between the increase in sintering temperature and the reduction of the contrast ratio. This trend can be attributed to three main phenomena: reduction of residual porosity due to the increase in sintering temperature; the decrease of the interface regions, i.e. grain boundary density in the volume of the specimens, due to the increase in the average size of the grains. These results are consistent with data reported in previous studies^{45,46}.

In a comparative analysis, samples G3 and G3Y showed less translucency than samples G5 and G5Y. This behavior is attributed to the predominance of the ZrO_2 -Cubic phase, isotropic, and of a phase with low tetragonality and consequently less anisotropic in the crystallographic composition of the material, tending to reduce losses due to birefringence.

Figure 9 shows the results measured for the contrast ratio, in groups of samples G3Y and G5Y, sintered at different temperatures, depending on the sample thickness.

The variations of the contrast ratio, depending on the thickness and sintering temperature, of the G3 and G5 samples are similar. However, the analysis of the results also points to a loss of translucency in the samples doped with Fe_2O_3 . Although the contrast ratio analysis considers only the variations in the luminance axis, the results indicate that, indirectly, the addition of Fe_2O_3 had a negative impact on the contrast ratio of all samples.

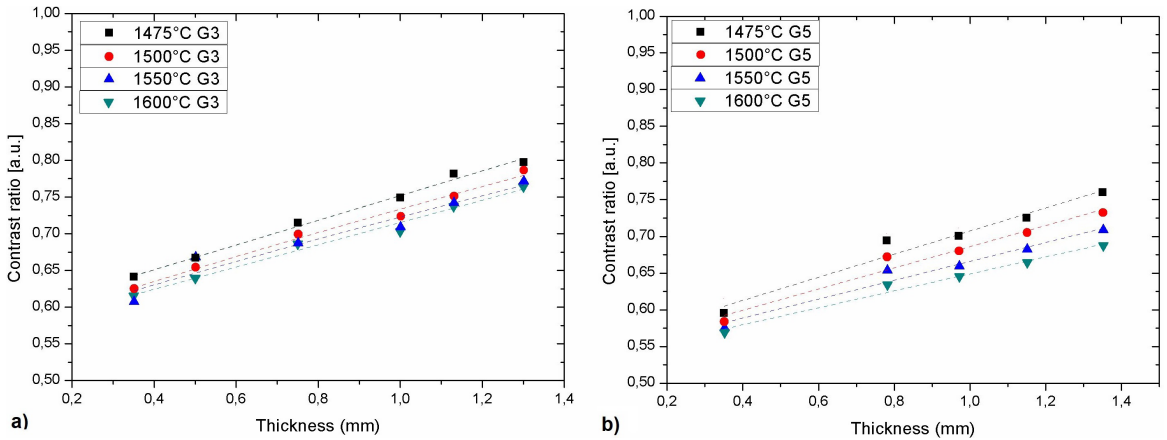


Figure 8. Contrast ratio CR of samples in regard to sample thickness: a) G3 and b) G5.

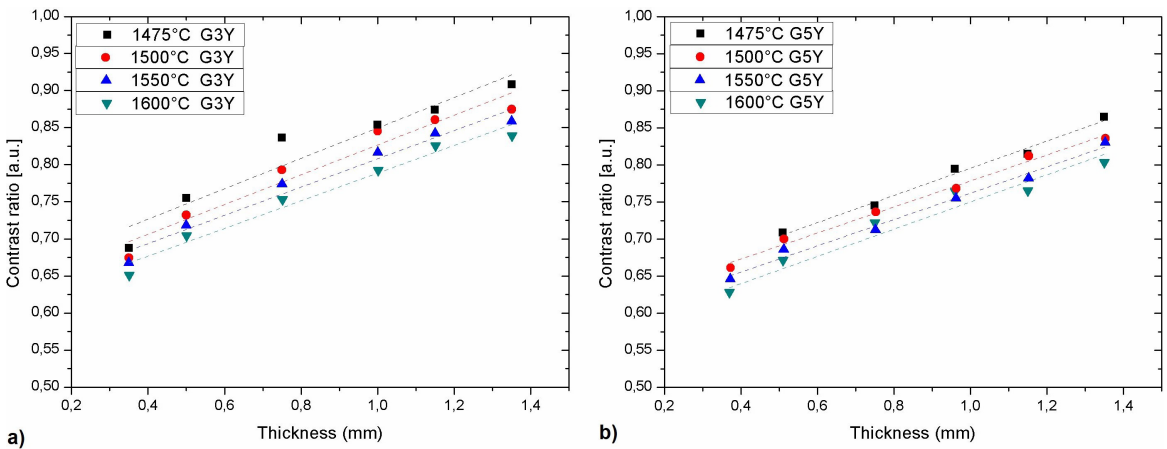


Figure 9. Contrast ratio of samples containing Fe₂O₃, depending on the thickness: a) G3Y and b) G5Y.

Another factor observed is that the addition of the coloring agent reduced the difference of the contrast ratio between samples G3Y and G5Y. While a contrast ratio difference of 9.5% can be observed between samples G3 and G5, sintered at 1600 °C, the difference between samples G3Y and G5Y, treated under the same conditions, was only 5, 5%, approximately.

Although there is no consensus as to the position occupied by Fe₂O₃, if dissolved in the ZrO₂ network or accumulated at grain boundaries, the scientific community agrees that the accumulation of impurities in the grain boundary causes loss of translucency, due to difference between the phase refraction indices^{12,47-49}.

The results of the contrast ratio also indicate that high sintering temperatures, above 1500 °C, reduces the contrast ratio. However, considering the results of porosity, in addition to the crystallographic parameters and the increase in the average grain size, it is plausible to assume that the contrast ratio is also impacted by the presence of residual porosity. Figure 10 illustrates some of the few cases in which residual porosity has been detected by SEM analysis.

For different starting materials, the pores detected were located at grain boundaries and were of an average size of less than 100 nm. According to the literature, the existence of residual porosity, even on a scale of less than

1%, significantly affects the optical properties of ceramic materials^{44,50}. According to the authors, the pore size is also an important factor, with a theoretical limit of 50 nm being proposed as the threshold in which the porosity affects the beam transmittance in the visible light spectrum.

3.5.2 Color difference (ΔE)

The differences in the yellow shades of the specimens G3Y and G5Y sintered at different temperatures, depending on the sample thickness, are shown in Figure 11.

The results indicate to an increase in the color difference as a function of the sintering temperature and the thickness of the specimens, with the specimens with the lowest Fe₂O₃ content showing the greatest variation. Some authors have developed studies focused on understanding the limit of human perception of color variations, within the limits of interest in restorative dentistry^{49,51-53}. In general, all authors detected an increase in color variation in samples submitted to a sintering cycle at a higher temperature, or for a longer time. However, none of the authors proved the mechanism responsible to cause this phenomenon. On the other hand, the literature converges regarding the perception limit of the human observer of color variation, establishing an ΔE of the order of 4 as being the perception limit, that is, color variations greater than that can be distinguished by the human eye.

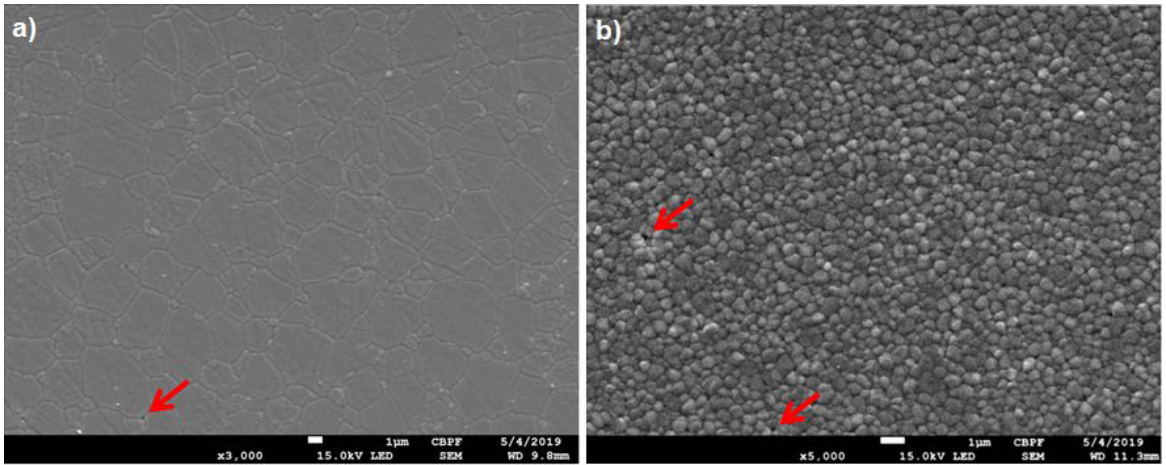


Figure 10. Examples of distribution and dimension of residual porosity in the analyzed specimens: a) G5 and b) G3.

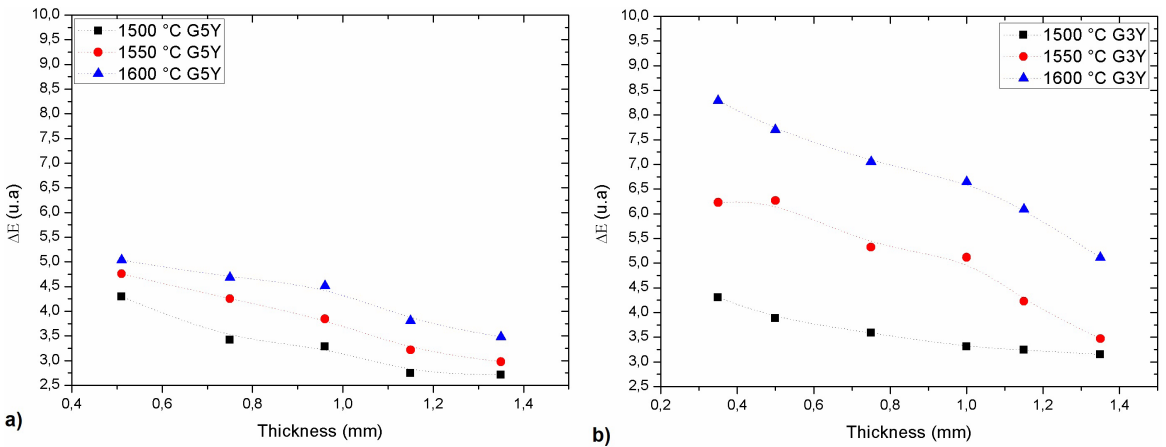


Figure 11. Color difference measured for the samples according to their thickness a) G5Y and b) G3Y.

Regarding these optical parameters, the G5Y samples with a thickness less than 0.75 mm and 1 mm, sintered at 1550°C or 1600°C, respectively, are above the perception limit. On the other hand, basically all G5Y samples sintered at the same temperatures are above the perception limit. Although a tendency was observed, the data obtained are insufficient to propose a mechanism to clarify this behavior.

4. Conclusions

The increase of the yttria content of the ZrO_2 powders from 3 mol% to 5 mol% resulted in significant changes of the phase composition and microstructure of the sintered materials. The variations in phase composition and microstructure of samples containing 3 or 5 mol% Y_2O_3 also reflect in the mechanical properties of the materials. Specifically, bending strength, as expressed by the characteristic strength σ_0 , decreased from about 1250 MPa to about 640 MPa when increasing the Y_2O_3 content from 3 to 5 mol%. Therefore, the ZrO_2 ceramics containing 5 mol% attend the requirements for the manufacture of dental prostheses of class 4 ($\sigma \geq 500$ MPa), such as three-element bridges involving molar restoration, but not the manufacture of class 5 dental prostheses ($\sigma \geq 800$ MPa), such as prostheses of four or more elements. These strength requirements are met by the ZrO_2 ceramics

containing 3 mol%, much higher than the requirements for class 5 prostheses. The Fe_2O_3 addition had no relevant effect on phase composition and microstructure. However, while the characteristic strength σ_0 has not been affected by the Fe_2O_3 addition, strength showed a larger scattering, as represented by a decreasing Weibull modulus m from 13.85 to 8.7 for samples stabilized with 3 mol% Y_2O_3 and from 12.6 to 8.7 for samples stabilized with 5 mol% Y_2O_3 .

Regarding the optical properties it has been found that all samples showed decreasing translucency and an increase in the contrast ratio with increasing sample thickness, while higher sinter temperatures reduced the of the contrast ratio. This reduction has been attributed to the smaller residual porosity and the reduction of grain boundaries by a larger grain growth at higher temperatures. It has also been observed that samples containing 3 mol% Y_2O_3 were less translucent compared to samples containing 5 mol% Y_2O_3 , with or without Fe_2O_3 additions, under otherwise identical sinter conditions. This behavior is attributed to the presence of the cubic, isotropic ZrO_2 phase besides a phase of low tetragonality in samples containing 5 mol% Y_2O_3 , reducing losses due to birefringence. Furthermore, an increase in the color difference as a function of the sintering temperature and the thickness of the specimens was observed, with the specimens with the lowest Fe_2O_3 content showing the greatest variation.

5. Acknowledgments

The authors would like to thank the LABNANO - CBPF for technical support during electron microscopy work, Furthermore, the authors thank FAPERJ (grant n° E26-201.476/2014), CNPq (grant n° 311119/2017-4 and grant n° 310237/2016-5) for financial support and Dr. Carlos Nelson Elias (IME-EB, Brazil) for 3D profilometry measurements.

6. References

- Kelly JR, Denry I. Stabilized zirconia as a structural ceramic: an overview. *Dent Mater.* 2008;24(3):289-98.
- Miyazaki T, Nakamura T, Matsumura H, Ban S, Kobayashi T. Current status of zirconia restoration. *J Prosthodont Res.* 2013;57(4):236-61.
- Sivaraman K, Chopra A, Narayan AI, Balakrishnan D. Is zirconia a viable alternative to titanium for oral implant? A critical review. *J Prosthodont Res.* 2018;62(2):121-33.
- Chevalier J, Gremillard I. Ceramics for medical applications: a picture for the next 20 years. *J Eur Ceram Soc.* 2009;29(7):1245-55.
- Tong H, Tanaka CB, Kaizer MR, Zhang Y. Characterization of three commercial Y-TZP ceramics produced for their high-translucency, high-strength and high-surface area. *Ceram Int.* 2016;42(1 Pt B):1077-85.
- Stawarczyk B, Frevert K, Ender A, Roos M, Sener B, Wimmer T. Comparison of four monolithic zirconia materials with conventional ones: contrast ratio, grain size, four-point flexural strength and two-body wear. *J Mech Behav Biomed Mater.* 2016;59:128-38.
- Kaplan M, Öztürk A, Park J. Production and characterization of yttria stabilized zirconia ceramic blocks for dental applications. In: 18th International Metallurgy and Materials Congress (IMMC 2016); 2016; Istanbul. Proceedings. Ankara: UCTEA; 2016. p. 324-7.
- Chavali R, Nejat AH, Lawson NC. Machinability of CAD-CAM materials. *J Prosthet Dent.* 2017;118(2):194-9.
- Kao CT, Tuan WH, Liu CY, Chen SC. Effect of iron oxide coloring agent on the sintering behavior of dental yttria-stabilized zirconia. *Ceram Int.* 2018;44(5):4689-93.
- Chevalier J. What future for zirconia as a biomaterial? *Biomaterials.* 2006;27(4):535-43.
- Camposilvan E, Leone R, Gremillard L, Sorrentino R, Zarone F, Ferrari M, et al. Aging resistance, mechanical properties and translucency of different yttria-stabilized zirconia ceramics for monolithic dental crown applications. *Dent Mater.* 2018;34(6):879-90.
- Zhang Y. Making yttria-stabilized tetragonal zirconia translucent. *Dent Mater.* 2014;30(10):1195-203.
- Apetz R, van Bruggen MPB. Transparent alumina: a light-scattering model. *J Am Ceram Soc.* 2003;86(3):480-6.
- Klimke J, Trunec M, Krell A. Transparent tetragonal yttria-stabilized zirconia ceramics: influence of scattering caused by birefringence. *J Am Ceram Soc.* 2011;94(6):1850-8.
- Yamashita I, Tsukuma K. Light scattering by residual pores in transparent zirconia ceramics. *J Ceram Soc Jpn.* 2011;119(1386):133-5.
- Yoshimura HN, Goldenstein H. Light scattering in polycrystalline alumina with bi-dimensionally large surface grains. *J Eur Ceram Soc.* 2009;29(2):293-303.
- dos Santos C, Rosa GO, Quintino MN, Rodrigues Pais Alves MF, Ribeiro S, Luis Melo-Silva C. Effect of surface finishing and thickness on the translucency of zirconia dental ceramics. *Ceram Int.* 2020;46(6):7748-55.
- Xiong Y, Fu Z, Pouchly V, Maca K, Shen Z. Preparation of transparent 3Y-TZP nanoceramics with no low-temperature degradation. *J Am Ceram Soc.* 2014;97(5):1402-6.
- Zhang F, Inokoshi M, Batuk M, Hadermann J, Naert I, Van Meerbeek B, et al. Strength, toughness and aging stability of highly-translucent Y-TZP ceramics for dental restorations. *Dent Mater.* 2016;32(12):e327-37.
- Jiang L, Liao Y, Wan Q, Li W. Effects of sintering temperature and particle size on the translucency of zirconium dioxide dental ceramic. *J Mater Sci Mater Med.* 2011;22(11):2429-35.
- ASTM: American Society for Testing and Material. ASTM C 373-88. Standard Test Method for Water Absorption, Bulk Density, Apparent Porosity and Apparent Specific Gravity of Fired Whiteware Products. West Conshohocken: ASTM; 2006.
- Peregrina-Barreto H, Terol-Villalobos IR, Rangel-Magdaleno JJ, Herrera-Navarro AM, Morales-Hernández LA, Manríquez-Guerrero F. Automatic grain size determination in microstructures using image processing. *Measurement.* 2013;46(1):249-58.
- ISO: International Organization for Standardization. ISO 6872:2015. Dentistry – Ceramic materials, Geneva: ISO; 2015.
- Quinn JB, Quinn GD. Review a practical and systematic review of Weibull statistics for reporting strengths of dental materials. *Dent Mater.* 2010;26(2):135-47.
- ISO: International Organization for Standardization. ISO 2471:2008: Paper and board -Determination of opacity (paper backing) - Diffuse reflectance method. Geneva: ISO; 2008.
- Guo F, Xiao P. Effect of Fe₂O₃ doping on sintering of yttria-stabilized zirconia. *J Eur Ceram Soc.* 2012;32(16):4157-64.
- Scott HG. Phase relationships in the zirconia-yttria system. *J Mater Sci.* 1975;10(9):1527-35.
- Krogstad JA, Lepple M, Gao Y, Lipkin DM, Levi CG. Effect of yttria content on the zirconia unit cell parameters. *J Am Ceram Soc.* 2011;94(12):4548-55.
- Lipkin DM, Krogstad JA, Gao Y, Johnson CA, Nelson WA, Levi CG. Phase evolution upon aging of air-plasma sprayed-t'-zirconia coatings: i-synchrotron x-ray diffraction. *J Am Ceram Soc.* 2012;96(1):290-8.
- Krogstad JA, Gao Y, Bai J, Wang J, Lipkin DM, Levi CG. In situ diffraction study of the high-temperature decomposition of t'-zirconia. *J Am Ceram Soc.* 2014;98(1):247-54.
- Matsui K, Horikoshi H, Ohmichi N, Ohgai M, Yoshida H, Ikuhara Y. Cubic-formation and grain-growth mechanisms in tetragonal zirconia polycrystal. *J Am Ceram Soc.* 2003;86(8):1401-8.
- Wang J, Stevens R. Review - zirconia-toughened alumina (ZTA) ceramics. *J Mater Sci.* 1989;24(10):3421-40.
- Basu B, Vleugels J, Biest OVD. Transformation behaviour of tetragonal zirconia: role of dopant content and distribution. *Mater Sci Eng A.* 2004;366(2):338-47.
- Xue W, Xie Z, Yi J, Chen J. Critical grain size and fracture toughness of 2 mol.% yttria-stabilized zirconia at ambient and cryogenic temperatures. *Scr Mater.* 2012;67(12):963-6.
- Shahmiri R, Standard OC, Hart JN, Sorrell CC. Optical properties of zirconia ceramics for esthetic dental restorations: a systematic review. *J Prosthet Dent.* 2018;119(1):36-46.
- Alves MFRP, Abreu LG, Klippel GGP, Santos C, Strecker K. Mechanical properties and translucency of a multi-layered zirconia with color gradient for dental applications. *Ceram Int.* 2021;47(1):301-9.
- Allemann JA, Michel B, Märki HB, Gauckler LJ, Moser EM. Grain growth of differently doped zirconia. *J Eur Ceram Soc.* 1995;15(10):951-8.
- Matsui K, Yamakawa T, Uehara M, Enomoto N, Hojo J. Mechanism of alumina-enhanced sintering of fine zirconia powder: influence of alumina concentration on the initial stage sintering. *J Am Ceram Soc.* 2008;91(6):1888-97.
- Matsui K, Yoshida H, Ikuhara Y. Review: microstructure-development mechanism during sintering in polycrystalline zirconia. *Int Mater Rev.* 2017;63(6):375-406.
- Holz L, Macias J, Vitorino N, Fernandes AJS, Costa FM, Almeida MM. Effect of Fe₂O₃ doping on colour and mechanical properties of Y-TZP ceramics. *Ceram Int.* 2018;44(15):17962-71.

41. Sedda M, Vichi A, Carrabba M, Capperucci A, Louca C, Ferrari M. Influence of coloring procedure on flexural resistance of zirconia blocks. *J Prosthet Dent.* 2015;114(1):98-102.
42. Apetz R, Bruggen MPB. Transparent alumina: a light-scattering model. *J Am Ceram Soc.* 2003;86(3):480-6.
43. Klimke J, Trunec M, Krell A. Transparent tetragonal yttria-stabilized zirconia ceramics: influence of scattering caused by birefringence. *J Am Ceram Soc.* 2011;94(6):1850-8.
44. Yamashita I, Tsukuma K. Light scattering by residual pores in transparent zirconia ceramics. *J Ceram Soc Jpn.* 2011;119(1386):133-5.
45. Ebeid K, Wille S, Hamdy A, Salah T, El-Etreby A, Kern M. Effect of changes in sintering parameters on monolithic translucent zirconia. *Dent Mater.* 2014;30(12):e-419-24.
46. Zhang F, Vanmeensel K, Batuk M, Hadermann J, Inokoshi M, Van Meerbeek B, et al. Highly-translucent, strong and aging-resistant 3Y-TZP ceramics for dental restoration by grain boundary segregation. *Acta Biomater.* 2015;16:215-22.
47. Zhang HB, Li ZP, Kim BN, Morita K, Yoshida H, Hiraga K, et al. Effect of alumina dopant on transparency of tetragonal zirconia. *J Nanomater.* 2012;2012:269064.
48. Kao CT, Tuan WH, Liu CY, Chen SC. Effect of iron oxide coloring agent on the sintering behavior of dental yttria-stabilized zirconia. *Ceram Int.* 2018;44(5):4689-93.
49. Koçak EF, Uçar Y, Kurtoğlu C, Johnston WM. Color and translucency of zirconia infrastructures and porcelain-layered systems. *J Prosthet Dent.* 2019;121(3):510-6.
50. Wagner A, Ratzker B, Kalabukhov S, Sokol M, Frage N. Residual porosity and optical properties of spark plasma sintered transparent polycrystalline cerium-doped YAG. *J Eur Ceram Soc.* 2018;39(4):1436-42.
51. Khashayar G, Bain PA, Salari S, Dozic A, Kleverlaan CJ, Feilzer AJ. Perceptibility and acceptability thresholds for colour differences in dentistry. *J Dent.* 2014;42(6):637-44.
52. Tabatabaian F, Dalirani S, Namdari M. Effect of thickness of zirconia ceramic on its masking ability: an in vitro study. *J Prosthodont.* 2019;28(6):666-71.
53. Giti R, Barfei A, Mohaghegh M. The influence of different shades and brands of resin-based luting agents on the final color of leucite-reinforced veneering ceramic. *Saudi Dent J.* 2019;31(2):284-9.